ELSEVIER

Journal of Nuclear Materials 266–269 (1999) 654–659

journal of nuclear materials

# Influence of $\mathbf{E} \times \mathbf{B}$ and $\nabla B$ drift terms in 2-D edge/SOL transport simulations

T.D. Rognlien *, G.D. Porter, D.D. Ryutov

*Lawrence Livermore National Laboratory, P.O. Box 808 (L-630), Livermore, CA 94551, USA*

**Abstract**

Classical particle drifts across the magnetic field can play an important role in tokamak edge-plasma transport. The relative influence of these terms is studied for self-consistent simulations by including them, together with anomalous diffusion transport, in a 2-D fluid model of edge-plasma transport for the DIII-D tokamak geometry. The drifts cause asymmetries in the plasma parameters between the inner and outer divertor regions which depend on the direction of the magnetic field, **B**. The basic results can be understood by dividing the drifts into three categories: diamagnetic, $\mathbf{E} \times \mathbf{B}$, and $\nabla B$. The dominant effect near the divertor plates is from the $\mathbf{E} \times \mathbf{B}$ drifts, while the weaker $\nabla B$ drifts cause an increase in the magnitude of the radial electric field inside the magnetic separatrix. The diamagnetic terms, defined here as divergence free, do not contribute to transport. 

*Keywords:* UEDGE; Divertor modeling; Electric field; $E \times B$ drift; Ion grad-B drift; DIII-D

## 1. Introduction

Classical particle drifts from $\mathbf{E} \times \mathbf{B}$ and $\nabla B$ (including curvature) drifts are believed to be important for understanding tokamak edge/scrape-off-layer (SOL) transport even in the presence of turbulent transport. For example, the asymmetry of the plasma density and temperature in front of the inner and outer divertor plates changes with the sign of the toroidal magnetic field, $B_t$ [1], and the power threshold for the L-H confinement transition often depends on the direction of $B_t$ [2]. There have been various analyses of the basic equations which describe these drift terms in toroidal geometry, e.g. [3,4]. However, careful assessment of their effects in 2-D transport codes has been lacking. Furthermore, it is important to have a valid model that calculates the electrostatic potential (and thus radial electric field, $E_r$) that extends across the magnetic separatrix into the core region. In this vicinity, shear in $E_r$ is believed to play an important role in suppressing edge turbulence.

In this paper, we focus on a study of the effects of the different classical drifts using the 2-D UEDGE transport code [5,6], including the calculation of $E_r$ on both sides of the separatrix [7,8]. The relative importance of the different drift terms, although not the details, can be predicted by simple arguments: First, the diamagnetic terms, defined here as being the divergence-free portion of the pressure-driven drift, give no transport as they cancel exactly in the transport equations; this is a well-known result which is sometimes overlooked. Second, the $\mathbf{E} \times \mathbf{B}$ drifts are larger than the $\nabla B$ drifts since the former scales as the inverse of the edge-plasma scale length while $\nabla B$ scales as the inverse major radius, $1/R$. Third, since the $\mathbf{E} \times \mathbf{B}$ drift is the same for ions and electrons, it generates no current; only the smaller $\nabla B$ drift enters the current continuity equation for the potential. The paper proceeds as follows: Section 2 gives a description of the transport equation, Section 3 presents the results of the UEDGE simulations, and Section 4 gives the conclusions.

* Corresponding author. Tel.: +1-925 422 9830; fax: +1-925 424 3484; e-mail: trognlien@1lnl.gov

0022-3115/99/$ – see front matter 
PII: S0022-3115(98)00835-6

## 2. Simulation model and transport equations

The UEDGE code solves for the plasma fluid equations in the 2-D poloidal plane, including a region inside the separatrix and extending to a wall bounding the SOL. The ($56 \times 28$) nonuniform mesh used is obtained from an MHD equilibrium for a DIII-D discharge (# 66832) as shown in Fig. 1. The direction of the core plasma current is into the plane of Fig. 1, giving a clockwise poloidal magnetic field in the SOL.

### 2.1. Plasma transport

Plasma equations are solved for the ion density, $n_i$, and ion parallel velocity $v_{i\|}$, and separate equations are used for the electron and ion temperatures, $T_e$ and $T_i$. All these equations have the form

$$\frac{\partial \psi_k}{\partial t} + \nabla \cdot (\alpha \mathbf{v} \psi_k - \mathbf{D}_k \cdot \nabla \psi_k) = F_k + S_k, \tag{1}$$

where $\psi_k$ represents variables of density, $n_i$ ($k = 1,\ \alpha = 1$), parallel momentum density, $n_i m_i v_{\|}$ ($k = 2,\ \alpha = 1$), and electron and ion thermal energy densities, $3n_e T_e/2$ and $3n_i T_i/2$, respectively ($k = 3,4,\ \alpha = 5/3$). Also $\mathbf{v}$ is the convection velocity from the parallel and cross-field drifts, $\mathbf{D}_k$ the diffusion tensor, $F_k$ a force term, and $S_k$ the source term.

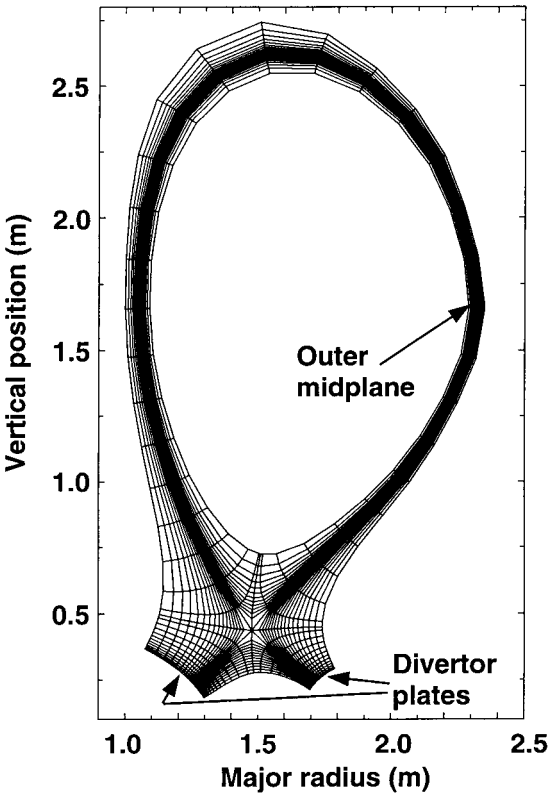


Fig. 1. The magnetic flux-surface mesh from DIII-D used in the UEDGE simulations.

Poloidal transport is a combination of the cross-field drifts described below and the geometrical projection of the parallel transport from Ref. [9], except that thermal flux limits are used. Radial transport also includes the cross-field drift components together with anomalous diffusion coefficients for density ($D$), parallel momentum ($\eta_{\|a}$, with subscript 'a' emphasizing anomalous), electron energy ($\chi_e$), and ion energy ($\chi_i$). The electrostatic potential is obtained from the current continuity equation described in more detail in Section 2.2. The neutral gas is described here by a diffusion model. Numerical methods and other details are available elsewhere [5,6].

If cross-field drifts are neglected, the convective velocity in Eq. (1) is taken as

$$\mathbf{v}_0 = v_{\|} \frac{B_p}{B} \hat{\mathbf{i}}_p - \frac{D}{n} \frac{\partial n}{\partial r} \hat{\mathbf{i}}_r, \tag{2}$$

where $B_p$ is the poloidal magnetic field, and $\hat{\mathbf{i}}_{p,r}$ are the unit vectors in the poloidal and radial directions, respectively. Note that in the continuity equation [$\psi_k = n_i$ in Eq. (1)], the diffusion term is actually represented through the diffusion term in $\mathbf{v}_0$.

Inclusion of the cross-field drifts can be accomplished by adding a second convective velocity such that $\mathbf{v} = \mathbf{v}_0 + \mathbf{v}_c$. To improve numerical accuracy, it is best to omit divergence-free convective fluxes from the outset as they should give zero contribution to the conservation equations [10]. The separation of particle fluxes into divergence-free terms and those from guiding-center motion is clearly reviewed by Chankin [3], and we use those results here. The guiding-center convection velocity assuming isotropic pressure for each species is

$$\mathbf{v}_c = \mathbf{v}_E + \mathbf{v}_{\nabla B} = \frac{\mathbf{E} \times \mathbf{B}}{B^2} + \frac{T}{qB^3} \mathbf{B} \times \nabla B + \frac{(T + m v_{\|}^2)}{qB^3} \mathbf{B} \times \mathbf{B} \nabla \cdot \left( \frac{\mathbf{B}}{B} \right), \tag{3}$$

where the first term on the right-hand side represents $\mathbf{v}_E$ and the remaining terms give the $\nabla B$ velocity $\mathbf{v}_{\nabla B}$. Here $E$ is the electric field, $T$ the electron or ion temperature, $q$ the particle charge, $m$ the mass, and $v_{\|}$ the parallel drift velocity. It should be emphasized that including $\mathbf{v}_c$ incorporates all cross-field drift terms in the conservation equations properly; one should not include any additional diamagnetic terms, i.e., neither the gyro-viscosity term in the momentum equation nor the energy diamagnetic terms [9].

### 2.2. Electrostatic potential equation

The potential is calculated from the current continuity equation obtained by subtracting the ion and

electron continuity equations and assuming quasineutrality ($n_i = n_e = n$), yielding

$$\nabla \cdot \mathbf{J} = 0. \tag{4}$$

Here we follow the description given in Ref. [7] with the generalization of including the currents from the $\nabla B$ terms in Eq. (3). (Note that $\mathbf{v}_E$ yields zero current.) We use the classical parallel current [9]

$$J_\parallel = \frac{en}{0.51 m_e v_e}\left(\frac{1}{n}\frac{\partial P_e}{\partial s} - e\frac{\partial \phi}{\partial s} + 0.71\frac{\partial T_e}{\partial s}\right), \tag{5}$$

where $s$ is the distance along $\mathbf{B}$, $P_e = nT_e$, and $v_e$ the electron collision frequency. While $J_\parallel$ dominates in the SOL, to move across the separatrix, we include a radial current driven by anomalous ion transport which in the thin SOL region can be approximated as [7]

$$J_r = e\left(\frac{1}{eB}\right)^2 \frac{\partial}{\partial r}\left[\eta_{\perp a}\frac{\partial}{\partial r}\left(\frac{1}{n}\frac{\partial P_i}{\partial r} + e\frac{\partial \phi}{\partial r}\right)\right], \tag{6}$$

where $\phi$ is the potential, $P_i = n_i T_i$, and $\eta_{\perp a} = m_i n_i D$ is an anomalous viscosity coefficient. The radial gradient of $B$ can be ignored as small in Eq. (6), so $B$ is taken outside the derivatives. However, gradients of $B$ do result in significant currents from $\mathbf{v}_{\nabla B}$ giving

$$\mathbf{J}_{\nabla B} = \frac{(P_e + P_i)}{B^3}\mathbf{B} \times \nabla B + \frac{(P_e + P_i + nm_i v_\parallel^2)}{B^3}\mathbf{B} \times \mathbf{B}\nabla \cdot \left(\frac{\mathbf{B}}{B}\right) \tag{7}$$

$$\approx (2P_e + 2P_i + nm_i v_\parallel^2)(\hat{\mathbf{i}}_R \times \hat{\mathbf{i}}_\phi)/BR, \tag{8}$$

where we assume singly charged ions; this is easily generalized to impurities. The unit vectors $\hat{\mathbf{i}}_{R,\phi}$ correspond to the direction of the major radius, $R$, and toroidal $B$-field, respectively. Eq. (8) is typically accurate for tokamaks, yielding a vertical current. To construct the total current, one does need to include the divergence-free current from Eq. (6) of Ref. [3], but we have no need for that here.

The current continuity equation thus becomes fourth order in the radial direction (from $J_r$) and second order in the poloidal direction (from $J_\parallel$). The sheath boundary conditions in the poloidal direction, including the cross-field drifts, are discussed in Ref. [11]. On the inner core boundary in the radial direction, we impose two boundary conditions: one is that the potential is constant on a flux surface, with the constant being supplied by requiring no radial current over the flux surface. The second condition is that the shape of the potential on the second set of cells in from the core boundary conform to that required for the electron temperature to be a flux function there as determined from parallel Ohm's law (5); the remaining constant is determined by setting the flux-surface averaged toroidal momentum to some input value (zero for the cases here). At the radial wall, simple boundary conditions making the first and second numerical derivatives of $\phi$ zero are used.

## 3. Simulation results

To study the effects of $\mathbf{E} \times \mathbf{B}$ and $\nabla B$ in a self-consistent simulation, we perform calculations for a parameter set typical of low-power DIII-D operation. The core-edge density is set to $2 \times 10^{19}$ m$^{-3}$ and the power

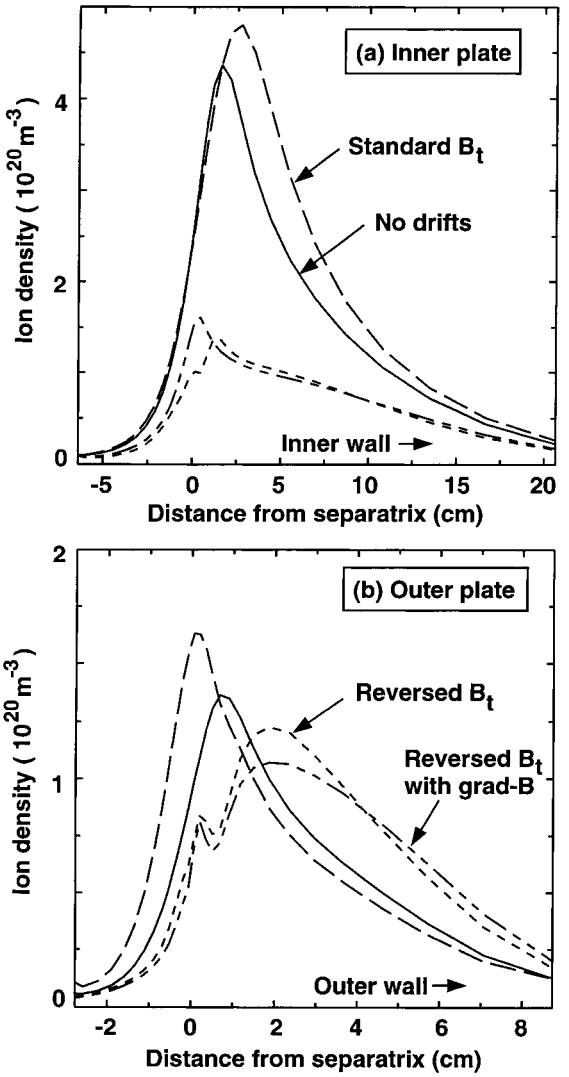


Fig. 2. Ion density at (a) inner divertor plate and (b) outer divertor plate for four cases: no cross-field drifts (solid line); $\mathbf{E} \times \mathbf{B}$ only for the standard toroidal B-field direction (long-dashed line); $\mathbf{E} \times \mathbf{B}$ only for reversed toroidal field (short-dashed line); and $\mathbf{E} \times \mathbf{B}$ and gradient-$B$ drifts for reversed toroidal field (dot–dashed line).

escaping from the core is 1.5 MW divided equally between ions and electrons. The plate recycling coefficient is 0.95, and the anomalous diffusion coefficients are all taken to be 0.5 $m^2/s$. The base-case sets both $\mathbf{v}_E$ and $\mathbf{v}_{\nabla B}$ to very small values which results in a detached divertor plasma on the inner plate with $T_e = 0.8$ eV and an attached plasma on the outer plate with peak $T_e = 5.4$ eV. The profiles of $n_i$ at each plate are shown as solid lines in Fig. 2.

### 3.1. Effect of $\mathbf{E} \times \mathbf{B}$

As mentioned earlier, the magnitude of the $\mathbf{E} \times \mathbf{B}$ velocity is much larger than that of the $\nabla B$ terms owing to the shorter scale-length of the potential compared to the magnetic field. Turning on the $\mathbf{E} \times \mathbf{B}$ velocity thus gives the dominant effect on plasma transport as shown in Fig. 2. Here the standard direction of $B_t$ is out of the plane of Fig. 1, giving the ion $\mathbf{v}_{\nabla B}$ velocity downward. Note from Fig. 2 that the profiles shift outward or inward in response to the radial drift caused by the poloidal electric field (always pointing toward the divertor plates).

The most dramatic effect of $\mathbf{E} \times \mathbf{B}$ in the divertor region is the strong drop in the density on the inner plate for reversed $B_t$ which results in loss of detachment on the inner divertor. The drop in $n_i$ can be understood by considering the vector plot of the ion flux shown in Fig. 3. Note the strong reversal of the flow under the X-point as $B_t$ changes sign; here the flow is dominated by the $\mathbf{E} \times \mathbf{B}$ drift from the large radial electric field that arises from the drop of $T_e$ in moving across the separatrix into the private flux region. Two diagnostics confirm that the particle flow under the X-point is very important here. First, consider three net ion-plus-neutral currents: that passing the X-point in the SOL toward the outer plate, $I_0$, that likewise directed toward the inner plate, $I_i$, and that passing under the X-point from inner plate to outer plate, $I_{pf}$. For the standard $B_t$, we find $(I_i, I_{pf}, I_0) = (0.13, -0.81, 1.6)$ kA, whereas for the reversed $B_t$, $(I_i, I_{pf}, I_0) = (1.6, 1.1, 0.05)$ kA. Clearly, $I_{pf}$ is comparable to the particle currents in the SOL and changes sign with $B_t$. Second, we insert a baffle vertically through the private flux region to the X-point for the reversed $B_t$ case; the solution then reverts to profiles very similar to the standard $B_t$ case (results not shown). The calculated effect of reversing $B_t$ is consistent with experimental results [1].

Note from Fig. 3 that the $\mathbf{E} \times \mathbf{B}$ induces rather complex flow patterns with flow reversal regions. Indeed, the self-consistent solution of the SOL plasma has many facets. Recently it has been shown [12] that even in a 1-D model including only poloidal drifts, but with temperature asymmetries, that supersonic solutions can arise where the density asymmetry can be enhanced in the direction opposite to the poloidal $\mathbf{E} \times \mathbf{B}$ velocity; the sign of this change is opposite to that found for the uniform temperature case.

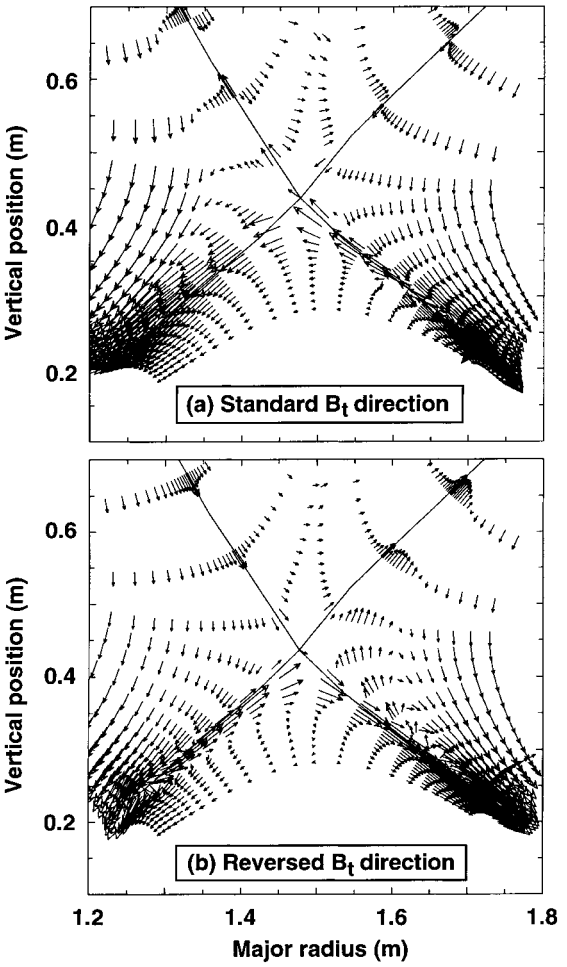


Fig. 3. Vectors of ion particle flux for (a) the standard direction of the toroidal magnetic field corresponding to the ion gradient-$B$ drift toward the X-point, and (b) the opposite direction for the toroidal field. The vector length is proportional to flux$^{0.5}$.

### 3.2. Effect of $\nabla B$

The effect of the $\nabla B$ velocities on plasma transport can be seen on the plate densities in Fig. 2 where the dot–dashed line gives the result of adding $\mathbf{v}_{\nabla B}$. The small change is a consequence of these drifts being small.

However, $\mathbf{v}_{\nabla B}$ does have a significant effect on the potential though their contributions to the net current via $\mathbf{J}_{\nabla B}$, especially in the core-edge region. Note from Eq. (7) that $\mathbf{J}_{\nabla B}$ does not explicitly depend on $\phi$, so it behaves like a source term in the equation used for the potential, $\nabla \cdot \mathbf{J}(\phi) = 0$, although the variables are coupled nonlinearly. The profiles of the radial electric field,

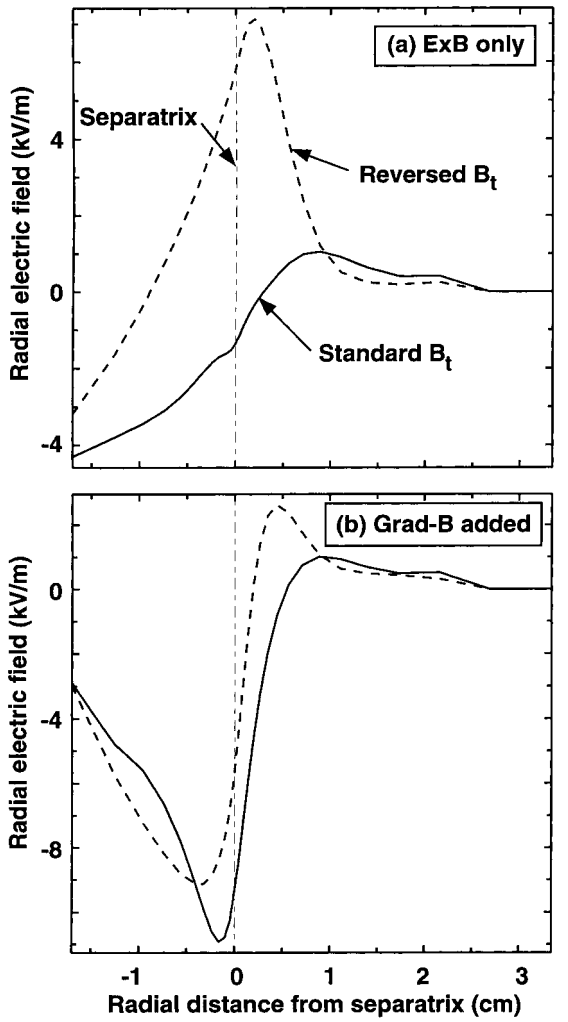


Fig. 4. Radial electric field at the outer midplane for (a) $\mathbf{E} \times \mathbf{B}$ drifts only, and (b) $\mathbf{E} \times \mathbf{B}$ and gradient-$B$ drifts together. The ion gradient-$B$ drifts are toward the X-point for the standard $B_t$ case.

$E_r$, are shown in Fig. 4 at the outer midplane without and with $\mathbf{J}_{\nabla B}$ added. The electric field is substantially changed near the separatrix and in the core region with $\mathbf{J}_{\nabla B}$. Note that well outside the separatrix, the parallel currents dominate the potential equation. The large radial shear seen in $E_r$ is believed important for suppressing edge turbulence, although quantitative evaluation of this process requires coupling this model with a turbulence simulation. Also, our simulations are done assuming no toroidal rotation at the core-edge boundary and are thus representative of DIII-D without strong neutral-beam injection which can cause toroidal rotation. Allowing finite toroidal velocity at the core-edge boundary changes $E_r$ inside the separatrix; quantitative evaluation of this effect will be presented in a subsequent paper [13].

Finally, the inclusion of $\mathbf{J}_{\nabla B}$ does change the current structure on the divertor plates. Although space does not permit a full discussion here, the currents at the plate in both standard and reversed $B_t$ cases are qualitatively similar to that measured on JET by Schaffer et al. [14], who also give an interpretation in terms of cross-field drifts. Even though the overall density profile on the plates are not very sensitive to $\nabla B$ effects (see Fig. 2), very near the separatrix, substantial currents do flow, especially for the reversed $B_t$ case where a strong negative current is found at the separatrix strike-point on both plates.

## 4. Summary

A study is made of the effect of classical cross-field drifts on plasma transport in the edge/SOL region of a tokamak using the DIII-D geometry as an example. The drifts can be separated into three categories: diamagnetic, $\mathbf{E} \times \mathbf{B}$, and $\nabla B$. The diamagnetic drift is defined here as the (large) divergence-free portion of the pressure-driven drift and thus contributes no net transport.

The $\mathbf{E} \times \mathbf{B}$ drift can be substantial in the edge region giving important contributions to particle transport. A large radial electric field exists in moving into the private flux region because of the rapid drop in the electron temperature there. The associated poloidal drift of private-flux region plasma is away from the outer plate and toward the inner plate for the ion gradient-$B$ drift toward the X-point. This particle transport further enhances the tendency from toroidal asymmetries for the inner plate to have higher plasma density and thus detach before the outer plate. Upon reversal of the toroidal field, $B_t$, the drifts reverse, and the plasmas at the inner and outer plates are much more similar. This behavior is consistent with the experimental observations reported in Ref. [1]. Because the $\mathbf{E} \times \mathbf{B}$ drift is the same for ions and electrons, it generates no net current and does not contribute directly to determining the electrostatic potential.

The $\nabla B$ drift is pressure-driven, but is typically smaller than the $\mathbf{E} \times \mathbf{B}$ drift by the ratio of $\Delta/R$, where $\Delta$ is the scrape-off layer width and $R$ is the major radius, but here ions and electrons drift in opposite directions; this drift thus first becomes important in the current continuity equation for determining the electrostatic potential. The perpendicular drift current is closed by the parallel current. In the core region, the current contribution from the $\nabla B$ drift increases the magnitude of $E_r$ and also its shear. In the SOL, the $\nabla B$ drift has a small effect on $E_r$ because there the current is dominated by the parallel electron dynamics.

## Acknowledgements

We gratefully acknowledge discussions with R.H. Cohen, N. Mattor, and M.E. Rensink. This work was performed under the auspices of the US Department of Energy by Lawrence Livermore National Laboratory under contract No. W-7405-Eng-48.

## References

[1] I.H. Hutchinson, B. LaBombard, J.A. Goetz et al., Plasma Phys. Contr. Fusion 37 (1995) 1389.
[2] K.H. Burrell, S. Ejima, D.P. Schissel et al., Phys. Rev. Lett. 59 (1987) 1432.
[3] A.V. Chankin, J. Nucl. Mater. 241–243 (1997) 199.
[4] V. Rozhansky, M. Tendler, Plasma rotation in tokamaks, in: B.B. Kadomtsev (Ed.), Reviews of Plasma Physics, vol. 19, Consultants Bureau, New York, 1996, p. 147.
[5] T.D. Rognlien, P.N. Brown, R.B. Campbell et al., Contr. Plasma Phys. 34 (1994) 362.
[6] G.R. Smith, P.N. Brown, R.B. Campbell, D.A. Knoll, P.R. McHugh, M.E. Rensink, T.D. Rognlien, J. Nucl. Mater. 220–222 (1995) 1024.
[7] T.D. Rognlien, D.D. Ryutov, Contrib. Plasma Phys. 38 (1998) 152.
[8] F.L. Hinton, Y.-B. Kim, Nucl. Fusion 34 (1994) 899.
[9] S.I. Braginskii, Transport processes in a plasma, in: Reviews of Plasma Physics, vol. 1, Consultants Bureau, New York, 1965, p. 205.
[10] G.J. Radford, A.V. Chankin, G. Corrigan et al., Contrib. Plasma Phys. 36 (1996) 187.
[11] R.H. Cohen, D.D. Ryutov, Phys. Plasma 2 (1995) 2011.
[12] R.H. Cohen, D.D. Ryutov, Bull. Am. Phys. Soc. 43 (1998) 1921; also to be published in Phys. Plasmas.
[13] T.D. Rognlien, D.D. Ryutov, N. Mattor, G.D. Porter, Bull. Am. Phys. Soc. 43 (1998) 1698; also to be published in Phys. Plasmas.
[14] M.J. Schaffer, A.V. Chankin, H.Y. Guo et al., Nucl. Fusion 37 (1997) 83.